Rock Mechanics and Rock Engineering
https://doi.org/10.1007/s00603-019-01920-7

ORIGINAL PAPER

# Cavity Expansion in Rock Masses Obeying the "Hoek–Brown" Failure Criterion

**Haythem Gharsallaoui**[1] · **Mustafa Jafari**[1] · **Alain Holeyman**[1]

Received: 8 February 2019 / Accepted: 16 July 2019


## Abstract
An unified approach is presented for the analysis of the expansion of both cylindrical and spherical cavities in an infinite elastic–perfectly plastic "Hoek–Brown" (H–B) material. The H–B failure criterion expressed in scaled form is adopted with a plastic flow rule characterized by a constant dilatancy angle $\psi$. Closed form expressions are given for the extent of the plastic region and the related stress. Solutions of the displacement field in the plastic region are provided based on both small-strain and large-strain theories. An original relationship between the cavity pressure and its expansion is derived. The developed closed-form solutions are validated employing the finite element method. For comparison purposes, an approximate solution is presented by neglecting the elastic strains in the plastic region which reveals that the assumption of no elastic strains does not influence the results for strong rocks in contrast with weak rocks. For practical purposes, design charts are provided allowing easy and accurate estimates of the limit pressure for cavity expansion in rock masses. The cavity expansion solution is finally validated against results obtained using the Finite Element modelling.

**Keywords** H–B failure criterion · Cylindrical cavity · Spherical cavity · Limit pressure · Plastic radius

### List of Symbols

| | |
|---|---|
| $r_i$ | Instant cavity radius |
| $r_{i0}$ | Original cavity radius |
| $r$ | Radial coordinate |
| $r_p$ | Plastic radius |
| $u$ | Radial displacement |
| $u_{\mathrm{EPB}}$ | Radial displacement at the elastic plastic boundary |
| $P_i$ | Internal cavity pressure |
| $P_y$ | Yield pressure |
| $P_0$ | Far field pressure |
| $P_{\lim}$ | Limit pressure |
| GSI | Geological strength index of the rock |
| $m_i$ | Strength parameter of the intact rock |
| $D$ | Disturbance factor of the rock |
| $s, a, m_b$ | Hoek–Brown-derived parameters |
| $E_i$ | Deformation modulus of the intact rock |
| $E_{rm}$ | Deformation modulus of the rock |
| $G$ | Shear modulus |
| $I_r$ | Rigidity index |
| $\varepsilon_r^e$ | Elastic radial strain |
| $\varepsilon_\theta^e$ | Elastic circumferential strain |
| $\varepsilon_r^p$ | Plastic radial strain |
| $\varepsilon_\theta^p$ | Plastic circumferential strain |
| $\sigma_1'$ | Major principal stress |
| $\sigma_3'$ | Minor principal stress |
| $\sigma_r$ | Radial stress |
| $\sigma_\theta$ | Circumferential stress |
| $\sigma_{ci}$ | Uniaxial compressive stress of the intact rock |
| $\sigma_c$ | Uniaxial compressive strength |
| $\sigma_t$ | Uniaxial tensile stress of the intact rock |
| $v$ | Poison ratio |
| $\psi$ | Dilatancy angle of the rock mass |
| $\omega$ | Dilatancy coefficient |

## 1 Introduction

The cavity expansion theory has been extensively developed and widely used to study a variety of practical geotechnical engineering problems. Among them, one can cite pile installation effects (Randolph and Wroth 1979), prediction of the bearing capacity of deep foundations

✉ Haythem Gharsallaoui
haythem.gharsallaoui@uclouvain.be

[1] Institute of Mechanics, Materials and Civil Engineering (iMMC), Civil and Environmental Engineering Department, Université Catholique de Louvain (UCLouvain), Place du Levant 1, 1348 Louvain La Neuve, Belgium

(Vesic 1973; Yasufuku and Hyde 1995), and interpretation of in situ tests such as pressuremeter tests PMT (Gibson and Anderson 1961) and cone penetration tests (Salgado et al. 1997). The main objective of this theory is to predict the stress and displacement fields around an expanding cavity. Most of analytical solutions are based on either small or large strain theories and the solution procedure for acquiring a complete pressure–expansion relationship varies. The small strain solution predicts an increasing internal pressure as the cavity expands, whereas the large strain solution predicts approaching a limit pressure at large expansions.

For cavities in rock masses, most practical applications still consider rock as a soil and predict their behavior using soil-related failure criteria such as the linear Mohr–Coulomb (M–C) criterion for which extensive literature is available (see Yu 2000 for topic review). Nevertheless, the non-linear Hoek–Brown (H–B) failure criterion represents the rock mass behavior more rigorously (Hoek and Brown 1980, 1997; Hoek et al. 2002). Since the introduction of the H–B criterion, most analyses have focused on cavity contraction rather than cavity expansion problems. The reason lies in the abundant practical applications such as tunneling and underground excavations, where it is crucial to estimate the tunnel convergence.

Earlier solutions for cavity contraction were developed by neglecting the contribution of elastic strains within the plastic region. These solutions for stress and displacement fields were provided for an elastic brittle plastic material obeying the 1980 H–B version (Brown et al. 1983; Wang 1996). Later on, Carranza-Torres and Fairhurst (1999) improved these solutions by considering the contribution of the elastic strains. They developed rigorous solutions for cavity contraction problem for a material obeying the 1997 H–B version with both associated and non-associated flow rules, but restricted to the perfectly elastic plastic behavior. Thereafter, their solutions were updated by Carranza-Torres (2004) for the generalized H–B version (2002). Despite the usefulness of their solutions, this last is not applicable to the brittle behavior of rock mass. Shortly thereafter, Sharan (2003, 2005, 2008) overcame this shortcoming by developing closed-form solutions for stress and displacement fields for cavity contraction problem in an elastic–brittle–plastic rock mass. The perfectly plastic analysis is conducted as a limiting case. Sharan's solutions (2003, 2005, 2008) are limited to the case of non-associated flow rule. Alternative solving method was proposed later by Serrano et al. (2011) whose solutions yield comparable results. Finally, Rojat et al. (2015) suggested a complementary analysis to the aforementioned work. They addressed the influence of the edges of the H–B failure envelope for an elastic–perfectly plastic material. Besides, they presented new closed-form solution for the case of an associated flow rule.

To the authors' knowledge, the cavity expansion problem in rock masses obeying the generalized H–B failure criterion (Hoek et al. 2002) has not been addressed. The development of complete rigorous solutions for stress and displacement fields is the main motivation of the present work. From a practical point of view, these solutions could be applied to analyses of driven, bored, and socketed piles in rock masses.

In this paper, the quasi-static expansion of both cylindrical and spherical cavities in rock masses is considered. The rock mass is treated as a perfect isotropic dilatant elastic plastic material obeying the generalized H–B failure criterion (Hoek et al. 2002). To simplify the governing equations of the problem, the generalized H–B expression is used in a "scaled"/non-dimensional form that led to considerable simplification in defining the elasto-plastic response of the rock mass. Besides, both small strain and large strain theories with non-associated flow rule are included for the study of the cavity expansion problem. That led to original solutions for stress and displacement fields. Moreover, a complete pressure–expansion relationship is provided. This relationship predicts limit pressure at large expansions. As a first aid to design engineers, charts are provided to estimate the limit pressure for the special case of non-dilatant rock mass for both cylindrical and spherical cavities.

## 2 "Hoek–Brown" (H–B) Material Behavior

### 2.1 Generalized H–B Failure Criterion

The H–B failure criterion is an empirical criterion developed through curve fitting of triaxial test data. The H–B criterion assumes isotropic rock and should only be applied to rock masses in which there are enough closely spaced discontinuities. In other words, the H–B failure criterion is valid either for intact rocks or for heavily jointed rock masses (i.e., sufficiently dense and randomly distributed joints). The H–B failure criterion was first introduced in 1980 with its latest update in 2002 (Hoek et al. 2002) defined as (positive compressive stresses):

$$\sigma_1' = \sigma_3' + \sigma_{ci}\left(m_b\frac{\sigma_3'}{\sigma_{\mathrm{ci}}} + s\right)^{\mathrm{a}}, \tag{1}$$

in which, $\sigma_1'$ and $\sigma_3'$ denote, respectively, the major and minor principal stresses at failure under triaxial loading conditions. $\sigma_{\mathrm{ci}}$ denotes the uniaxial compressive strength of the intact rock ranging from 1 (weak rock) to 100 [MPa] (strong rock). The strength parameters $m_b$, $s$, and $a$ describe the rock mass strength characteristics and they depend on the Geological Strength Index GSI, the disturbance factor $D$, and the intact frictional strength parameter $m_i$. The strength parameters are defined by:

$$m_b = m_i \exp\left(\frac{\text{GSI} - 100}{28 - 14D}\right), \tag{2}$$

$$s = \exp\left(\frac{\text{GSI} - 100}{9 - 3D}\right), \tag{3}$$

$$a = \frac{1}{2} + \frac{1}{6}\left(\exp\left(-\frac{\text{GSI}}{15}\right) - \exp\left(-\frac{20}{3}\right)\right). \tag{4}$$

As can be seen in Fig. 1, the frictional strength parameter $m_b$ increases gradually with increasing GSI values until reaching the value of $m_i$ when GSI equals 100.

The relationships between GSI and both $a$ and $s$ are also shown in Fig. 1. For GSI < 40, $s$ becomes very small and $a$ is slightly larger than 0.5. For GSI > 40, $a$ is approximately 0.5 while $s$ increases exponentially with increasing GSI value until reaching 1 when GSI equals 100.

On the other hand, the uniaxial compressive strength of the rock mass is obtained by setting $\sigma_3' = 0$ in Eq. (1), given in the following equation:

$$\text{UCS} = \sigma_c = \sigma_{ci}.s^a, \tag{5}$$

while the uniaxial tensile strength of the rock mass $\sigma_t$ is obtained by setting $\sigma_1' = 0$ and $\sigma_3' = \sigma_t$ in Eq. (1), resulting in the following equation that should be solved by a numerical tool:

$$\frac{\sigma_t}{\sigma_{ci}} + (m_b\frac{\sigma_t}{\sigma_{ci}} + s)^a = 0. \tag{6}$$

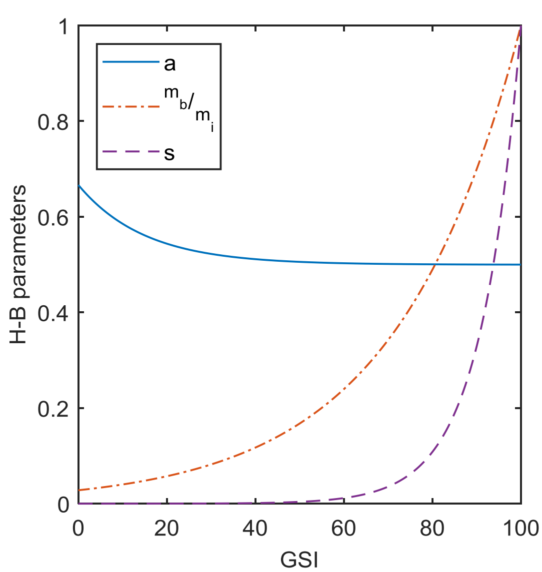


**Fig. 1** H–B parameters as a function of GSI for $D = 0$

- Elastic Properties

The deformation modulus is expressed for a H–B material as a function of the intact rock modulus $E_i$[MPa], GSI, and D as follows (Hoek and Diederichs 2006):

$$\frac{E_{\text{rm}}}{E_i} = \left(0.02 + \frac{1 - D/2}{1 + \exp\left(\frac{60+15.D-\text{GSI}}{11}\right)}\right)[\text{MPa}]. \tag{7}$$

Vásárhelyi (2009) provides an estimate of the Poisson's ratio as a function of GSI and $m_i$:

$$\nu = -0.002.\text{GSI} - 0.003.m_i + 0.457. \tag{8}$$

## 2.2 Scaled H–B Failure Criterion

The H–B failure criterion expression (Eq. 1) defines the relationship between minor and major principal stresses depending on four independent parameters, which can be reduced to a single one using a "scaled" form of the criterion. The suggested transformation involves dividing Eq. (1) by $\sigma_{ci}m_b^\beta$ and adding the term $\left(s/m_b^{\beta/a}\right)$ to both sides. With these manipulations, the H–B failure criterion expression becomes:

$$\frac{\sigma_1'}{\sigma_{ci}m_b^\beta} + \frac{s}{m_b^{\beta/a}} = \frac{\sigma_3'}{\sigma_{ci}m_b^\beta} + \frac{s}{m_b^{\beta/a}} + \left(\frac{\sigma_3'}{\sigma_{ci}m_b^\beta} + \frac{s}{m_b^{\beta/a}}\right)^a, \tag{9}$$

where $\beta$ is a constant solely depending on the exponent $a$ and that can be expressed as follows:

$$\beta = \frac{a}{1 - a}. \tag{10}$$

Thus, the scaled (non-dimensional) minor and major principal stresses are defined naturally as,

$$\sigma_j^* = \frac{\sigma_j'}{\sigma_{ci}m_b^\beta} + \frac{s}{m_b^{\beta/a}}; \quad j = \{1, 3\}. \tag{11}$$

When expressed in terms of $\sigma_1^*$ and $\sigma_3^*$, the H–B failure criterion permits a simplified and normalized treatment of the rock mass failure condition.

Thanks to such a scaling, the H–B failure criterion is formally simplified as follows:

$$\sigma_1^* = \sigma_3^* + \left(\sigma_3^*\right)^a. \tag{12}$$

It should be noted that Londe (1988) made a similar transformation for a rock obeying the 1997 H–B version (Hoek and Brown 1997) with the assumption that the exponent $a$ is equal to 0.5. However, the suggested scaling procedure applies to any value of the exponent $a$ according the 2002 version of the generalized H–B failure criterion (Hoek et al. 2002). Figure 2 depicts the H–B criterion under its scaled form for three GSI values.

## 3 Problem Statement

Both cylindrical and spherical cavities in an infinite elastic–perfectly plastic H–B material are considered. The geometry of the problem and the boundary conditions are depicted in Fig. 3.

Let $r_i$ be the internal radius of the cavity and $P_0$ the far field isotropic pressure. Let $P_i$ be the internal pressure applied on the cavity wall that increases monotonically from its initial value $P_0$. As the internal pressure $P_i$ increases, the rock mass will initially behave in an elastic manner, until reaching a yield pressure $P_y$. When the internal pressure $P_i$ exceeds $P_y$, a plastic region will start spreading from $r_i$ to a "plastic" radius $r_p$. The remainder of the domain ($r \geq r_p$) belongs to the elastic region.

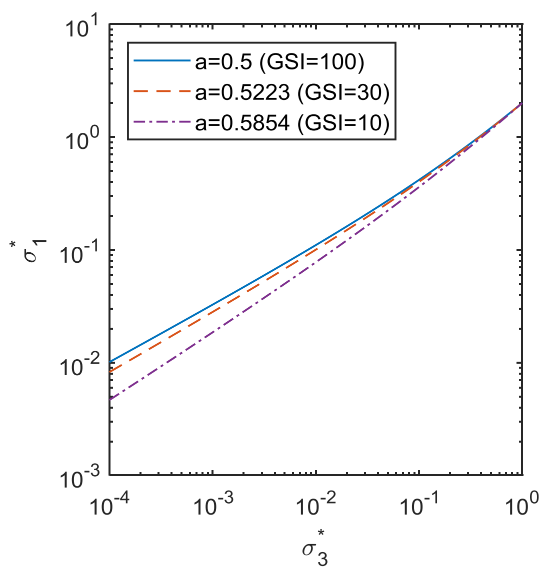


**Fig. 2** H–B failure criterion yield surface (scaled form) for three values of GSI

The equation of equilibrium for the cavity problem is expressed in terms of radial and circumferential stresses as follows:

$$\frac{\mathrm{d}\sigma_r}{\mathrm{d}r} + k\frac{\sigma_r - \sigma_\theta}{r} = 0, \tag{13}$$

which can be further written, in scaled form as per Eq. (11), as:

$$\frac{\mathrm{d}\sigma_r^*}{\mathrm{d}r} + k\frac{\sigma_r^* - \sigma_\theta^*}{r} = 0. \tag{14}$$

Here, $k$ is a coefficient equal to 1 in case of a cylindrical cavity, to 2 in case of a spherical cavity.

Note that major and minor principal stresses are assumed to be equal to the radial and circumferential stresses, respectively, i.e.,

$$\sigma_1 = \sigma_r, \tag{15}$$

$$\sigma_3 = \sigma_\theta. \tag{16}$$

It should be emphasized that the analytical study described in this paper is conducted based on the scaled form of the H–B failure criterion presented in Sect. 1.2. That means that pressures are expressed, in scaled form, as

$$P_c^* = \frac{P_c}{\sigma_{ci} m_b^\beta} + \frac{s}{m_b^{\beta/a}}. \tag{17}$$

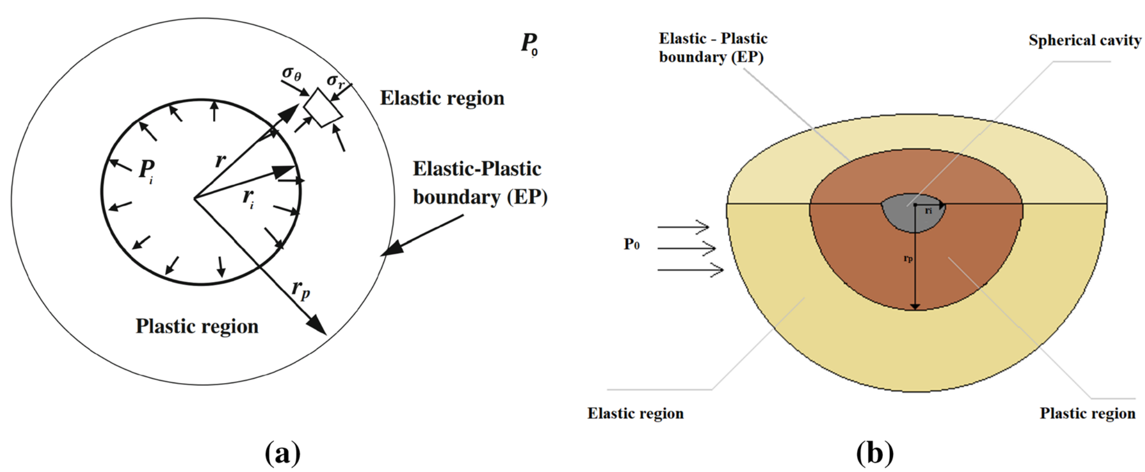


**Fig. 3** Geometry of the problem and boundary conditions—Cylindrical (**a**) and spherical (**b**) cavities (after Hamdi 2016)

With the index $c$ = "0" or "$i$" or "$y$ denoting, respectively, the far field condition, the cavity wall, and the yield conditions. The normalized pressure will have an asterisk as superscript. For the sake of brevity, the term "scaled" will be mostly dropped when referring to a scaled variable unless stated otherwise.

In what follows, solutions of cavity expansion problems are provided in the elastic and plastic regions.

## 4 Elastic Solution ($P_i < P_y$)

In this section, the classical elastic problem of both cylindrical and spherical cavity expansions is considered and that when the internal pressure $P_i$ applied on the cavity wall does not exceed the yield pressure $P_y$. Since the solution for this problem is well known, only, main results are presented hereafter.

Considering the boundary conditions ($\sigma_r^*\left(r = r_i\right) = P_i^*$ and $\sigma_r^*(r = \infty) = P_0^*$), the radial and circumferential stresses are given, as:

$$\sigma_r^*(r) = P_0^* + \left(P_i^* - P_0^*\right)\left(\frac{r_i}{r}\right)^{k+1}, \tag{18}$$

$$\sigma_\theta^*(r) = P_0^* - \frac{1}{k}\left(P_i^* - P_0^*\right)\left(\frac{r_i}{r}\right)^{k+1}. \tag{19}$$

On the other hand, the radial dfvisplacement $u$ can be determined from the radial or the circumferential strains as follows:

$$\varepsilon_r = \varepsilon_r^e = -\frac{\mathrm{d}u}{\mathrm{d}r}, \tag{20}$$

$$\varepsilon_\theta = \varepsilon_\theta^e = -\frac{u}{r}, \tag{21}$$

where $\varepsilon_r^e$ and $\varepsilon_\theta^e$ are given as follows:

$$\varepsilon_r^e = \frac{1}{2I_r(1+\nu)^{k-1}}\left((1+\nu(k-2))\left(\sigma_r^* - P_0^*\right) - k\nu\left(\sigma_\theta^* - P_0^*\right)\right), \tag{22}$$

$$\varepsilon_\theta^e = \frac{1}{2I_r(1+\nu)^{k-1}}\left((1-\nu)\left(\sigma_\theta^* - P_0^*\right) - \nu\left(\sigma_r^* - P_0^*\right)\right) \tag{23}$$

in which, $\nu$ is the Poisson's ratio. $I_r$ is the rigidity index of the rock mass and it is expressed as

$$I_r = \frac{G}{\sigma_{ci} m_b^\beta}. \tag{24}$$

Substituting Eqs. (18) and (19) into one of the above equations results in the following radial displacement:

$$u(r) = -r\varepsilon_\theta^e = \frac{1}{2kI_r}\left(P_i^* - P_0^*\right) r_i \left(\frac{r_i}{r}\right)^k. \tag{25}$$

## 5 Elastic–Perfectly Plastic Solution ($P_i > P_y$)

When the internal pressure $P_i$ applied on the cavity wall reaches the yield pressure $P_y$, the stress of the rock mass at cavity face will satisfy the failure criterion. Thus, substituting Eqs. (18) and (19) into Eq. (12), the yield pressure should satisfy the following expression:

$$\left(P_y^* - P_0^*\right) = -\frac{1}{k}\left(P_y^* - P_0^*\right) + \left[P_0^* - \frac{1}{k}\left(P_y^* - P_0^*\right)\right]^a. \tag{26}$$

The yield pressure depends only on the far field pressure $P_0^*$ and the exponent $a$. The above equation provides an explicit solution when $a = 0.5$ and the following hold:

$$P^*_{y_{|a=0.5}} = P_0^* + \frac{k\left(\sqrt{4P_0^*(k+1)^2 + 1} - 1\right)}{2(k+1)^2}. \tag{27}$$

When $a \neq 0.5$, there is no explicit solution and Eq. (25) should be solved numerically. Otherwise, one can resort to the Newton–Raphson algorithm (Ypma 1995) starting from the value obtained when $a = 0.5$ to provide an approximate solution with one simple iteration. Thus,

$$P_y^* \cong P_0^* + \Delta P^*_{y_{|a=0.5}} - \frac{\Delta P^*_{y,a=0.5}\left(1+\frac{1}{k}\right) - \left(P_0^* - \frac{\Delta P^*_{y,a=0.5}}{k}\right)^a}{\left(1+\frac{1}{k}\right) + \frac{a}{k}\left(P_0^* - \frac{\Delta P^*_{y,a=0.5}}{k}\right)^{a-1}}, \tag{28}$$

where $\Delta P^*_{y_{|a=0.5}} = P^*_{y_{|a=0.5}} - P_0^*$ is the net yield pressure.

The evolution of $P_y^*$ as a function of $P_0^*$ is shown in Fig. 4. As can be seen, $P_y^*$ is equal to $2P_0^*$ and $3P_0^*$ when $P_0^* \to 0$

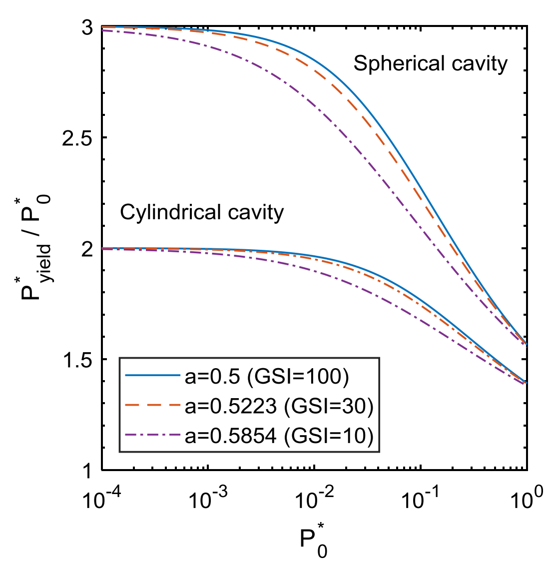


**Fig. 4** Scaled yield pressure

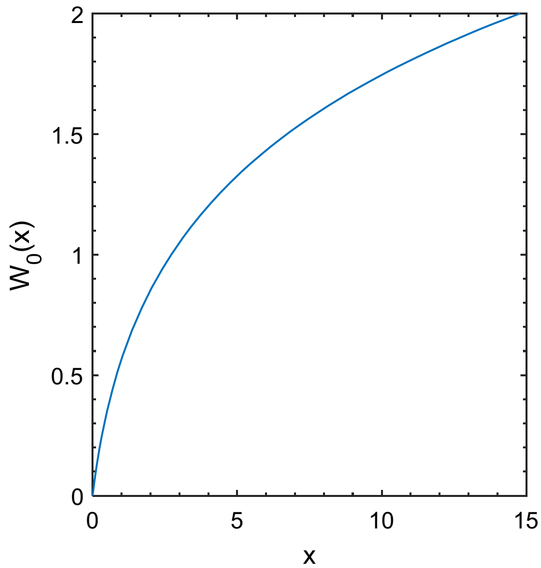


**Fig. 5** Zeroth branch of the Lambert $W$-function

for the cylindrical and spherical cavities, respectively. Secondly, the scaled yield pressure is relatively constant when GSI > 30 since the exponent $a \cong 0.5$ in that range.

When the internal pressure $P_i$ exceeds $P_y$, a plastic region starts spreading from $r_i$ to the plastic radius $r_p$. The remainder of the domain ($r \geq r_p$) belongs to the elastic region. The latter is first studied before investigating the plastic region.

### 5.1 Elastic Region ($r \geq r_p$)

To determine the stress and displacement fields in the elastic region, the relevant boundary conditions are taken into account: $\sigma_r^*(r = r_p) = P_y^*$ and $\sigma_r^*(r = \infty) = P_0^*$. The radial and circumferential stresses are expressed as:

$$\sigma_r^* = P_0^* + \left(P_y^* - P_0^*\right)\left(\frac{r_p}{r}\right)^{k+1}, \tag{29}$$

$$\sigma_\theta^* = P_0^* - \frac{1}{k}\left(P_y^* - P_0^*\right)\left(\frac{r_p}{r}\right)^{k+1}. \tag{30}$$

On the other hand, the total strains are written as functions of elastic and plastic strains as follows:

$$\varepsilon_r = \varepsilon_r^e + \varepsilon_r^p, \tag{31}$$

$$\varepsilon_\theta = \varepsilon_\theta^e + \varepsilon_\theta^p, \tag{32}$$

where $\varepsilon_r^e$ and $\varepsilon_\theta^e$ are, respectively, the radial and the circumferential elastic strains given as per Eqs. (22) and (23). $\varepsilon_r^p$ and $\varepsilon_\theta^p$ denote, respectively, the radial and the circumferential plastic strains. They will be evaluated in the next Sect. 5.2.

By substituting Eqs. (29) and (30) into Eqs. (22) and (23), elastic strains are given, for both cylindrical and spherical cavities, as follows:

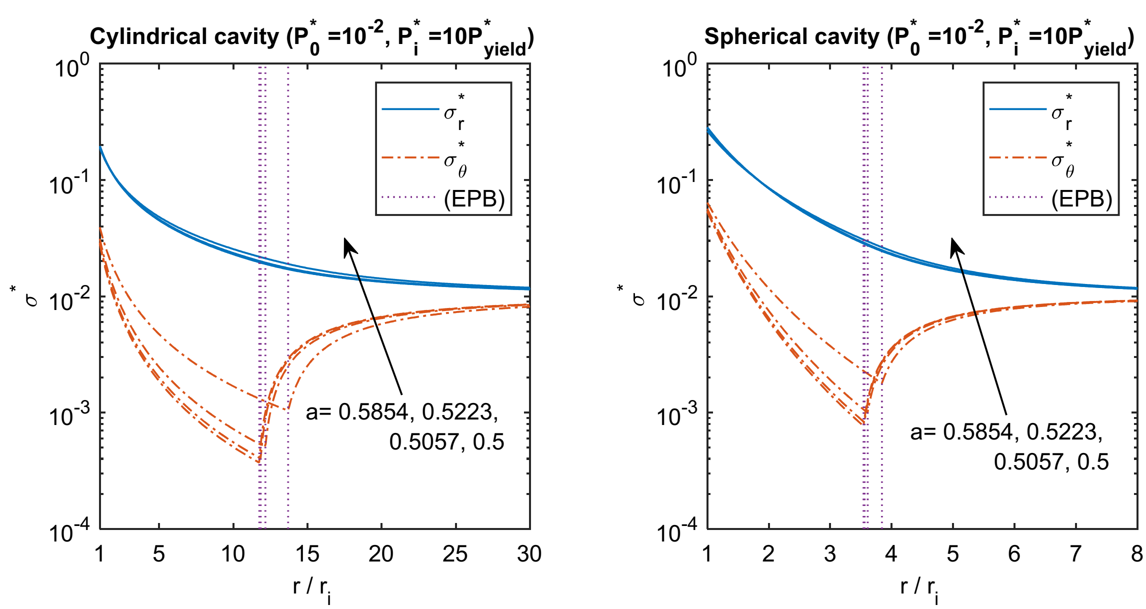


**Fig. 6** Radial distribution of radial and circumferential stresses for different values of the exponent a

$$\varepsilon_r^e = \frac{1}{2I_r}\left(P_y^* - P_0^*\right)\left(\frac{r_p}{r}\right)^{k+1}, \tag{33}$$

$$\varepsilon_\theta^e = \frac{1}{2kI_r}\left(P_0^* - P_y^*\right)\left(\frac{r_p}{r}\right)^{k+1}. \tag{34}$$

Infinitesimal strain can be written in terms of radial displacement $u$ as follows:

$$\varepsilon_r = -\frac{\mathrm{d}u}{\mathrm{d}r} \tag{35}$$

$$\varepsilon_\theta = -\frac{u}{r} \tag{36}$$

Thus, the radial displacement $u$ can be evaluated using one of the above equations as follows:

$$u = -r\varepsilon_\theta^e = \frac{1}{2kI_r}\left(P_y^* - P_0^*\right)r_p\left(\frac{r_p}{r}\right)^k, \tag{37}$$

which can be further written as:

$$u = u_{\mathrm{EPB}}\left(\frac{r_p}{r}\right)^k. \tag{38}$$

Here, $u_{\mathrm{EPB}} = \frac{1}{2\mathrm{k}I_r}\left(P_y^* - P_0^*\right).r_p$ is the radial displacement at the elastic–plastic boundary (EPB).

## 5.2 Plastic Region ($r_i \le r \le r_p$)

Determining the stress and displacement field in the plastic region for the nonlinear H–B criterion is quite involved as presented hereafter.

### 5.2.1 Stress Field

By substituting the scaled H–B failure criterion expression given in Eq. (12) into the expression of equilibrium for cavity expansion given in Eq. (14), the following differential equation of the scaled circumferential stress holds:

$$\frac{\mathrm{d}\sigma_\theta^*}{\mathrm{d}r} + \frac{\mathrm{d}\left(\sigma_\theta^*\right)^a}{\mathrm{d}r} + k\frac{\left(\sigma_\theta^*\right)^a}{r} = 0. \tag{39}$$

The general solution of the above first-order nonlinear differential equation can be written as:

$$\sigma_\theta^*(r) = \left[aW_0\left(\frac{C_1}{r^{\frac{k}{\beta}}}\right)\right]^{\beta/a}, \tag{40}$$

and subsequently, the scaled radial stress is expressed as per Eq. (12) as follows:

$$\sigma_r^*(r) = \left[aW_0\left(\frac{C_1}{r^{\frac{k}{\beta}}}\right)\right]^{\beta/a} + \left[aW_0\left(\frac{C_1}{r^{\frac{k}{\beta}}}\right)\right]^{\beta}, \tag{41}$$

where $C_1 i$ s a constant. $W_0$ is the $0^{\text{th}}$ branch of the Lambert $W$-function (Omega function). Lambert $W$-function is the solution of the equation $x = W(x)e^{W(x)}$. The branch $W_0(x)$ is depicted in Fig. 5.

To simplify the mathematical expressions, the following change of variable will be used:

$$R = C_1 r^{-\frac{k}{\beta}}, \tag{42}$$

which allows Eqs. (40) and (41) to be reduced to

$$\sigma_\theta^*(R) = \left[aW_0(R)\right]^{\beta/a}, \tag{43}$$

$$\sigma_r^*(R) = \left[aW_0(R)\right]^{\beta/a} + \left[aW_0(R)\right]^{\beta}. \tag{44}$$

Based on the hypothesis of the continuous radial stress at the (EPB) and knowing that an internal scaled pressure $P_i^*$ is exerted at the cavity wall, i.e.,

$$P_y^* = \left[aW_0\left(R_p\right)\right]^{\beta/a} + \left[aW_0\left(R_p\right)\right]^{\beta}, \tag{45}$$

$$P_i^* = \left[aW_0\left(R_i\right)\right]^{\beta/a} + \left[aW_0\left(R_i\right)\right]^{\beta}; \tag{46}$$

the plastic radius $r_p$ can be calculated once Eqs. (45) and (46) are solved for $R_p = C_1 r_p^{-\frac{k}{\beta}}$ and $R_i = C_1 r_i^{-\frac{k}{\beta}}$, respectively. Thus, the normalized plastic radius $r_p/r_i$ is simply given by:

$$\frac{r_p}{r_i} = \left(\frac{R_i}{R_p}\right)^{\frac{\beta}{k}}. \tag{47}$$

When $a = 0.5$, a closed-form solution of the plastic radius can be provided:

$$\left(\frac{r_p}{r_i}\right)_{a=0.5} = \left(\frac{\sqrt{4P_i^*+1}-1}{\sqrt{4P^*_{y|a=0.5}+1}-1}\,\frac{e^{\sqrt{4P_i^*+1}-1}}{e^{\sqrt{4P^*_{y|a=0.5}+1}-1}}\right)^{\frac{1}{k}}. \tag{48}$$

When $a \ne 0.5$, there is no closed-form solution for the plastic radius and Eqs. (45) and (46) should be solved numerically.

The radial distribution of radial and circumferential stresses for $a = 0.5854, 0.5223, 0.5057$, and $0.5$ (i.e., $\mathrm{GSI} = 10, 30, 50$, and $100$) are depicted in Fig. 6 for both cylindrical and spherical cavities. It is observed that, unlike for the radial stress, there is a significant difference of circumferential stress values when $GSI < 30$. As shown,

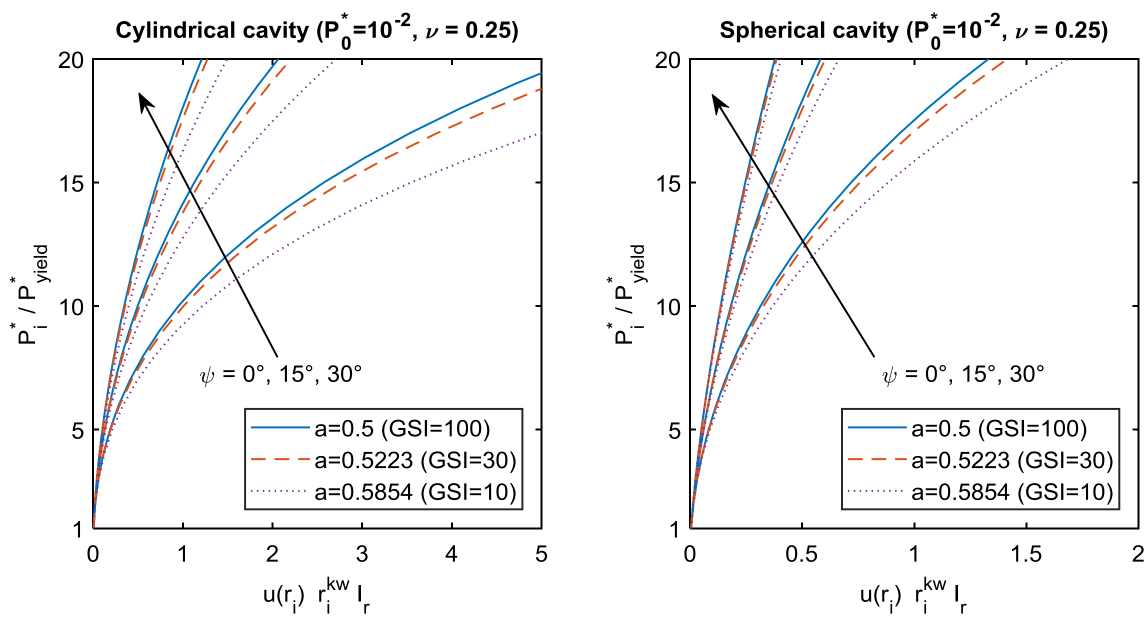


**Fig. 7** Typical pressure–displacement curves employing the small strain theory (SST)

increasing $a$ values (i.e., decreasing GSI values) result in a larger plastic zone.

### 5.2.2 Displacement Field

To determine the displacement field in the plastic zone, a plastic flow rule is needed. Thus, a non-associated flow rule with a constant dilatancy angle $\psi$ of the H–B material is adopted as:

$$\varepsilon_r^p + k\omega\varepsilon_\theta^p = 0, \tag{49}$$

in which, $\omega = \frac{1-\sin(\psi)}{1+\sin(\psi)}$.

The above relationship between plastic strains can be further expressed as per Eqs. (31) and (32) as:

$$\varepsilon_r + k\omega\varepsilon_\theta = \varepsilon_r^e + k\omega\varepsilon_\theta^e. \tag{50}$$

In above equations, the strain–displacement relationship depends on whether a small deformation or large deformation theory is adopted. Although Vrakas (2016) provided a relationship between small and large strain solutions for general cavity expansion problems in elasto-plastic Mohr–Coulomb material, his solution has limitations due to many simplifying assumptions that facilitated his derivation. The main restrictive one was disregarding elastic strains within the plastic zone. Such assumption influences the results significantly. That is why, two different resolution strategies are adopted separately hereinafter.

(a) Small Strain Theory (SST)

In small deformation analyses, the fact that displacements modify the position of material points is ignored. Thus, the SST is only valid for small expansions. In this case, strains can be expressed in terms of radial displacement $u$ as follows:

$$\varepsilon_r = -\frac{du}{dr}, \tag{51}$$

$$\varepsilon_\theta = -\frac{u}{r} \tag{52}$$

Substituting the above equations into Eq. (50) combined with Eqs. (22) and (23) results in the following differential equation of the radial displacement:

$$\frac{du}{dr} + k\omega\frac{u}{r} + D_1\left(\sigma_\theta^* - P_0^*\right) + D_2\left(\sigma_\theta^*\right)^a = 0, \tag{53}$$

where $D_1$ and $D_2$ are two dimensionless coefficients defined as follows:

$$D_1 = \frac{(1+k\omega)(1-2\nu)}{2I_r(1+\nu)^{k-1}}, \tag{54}$$

$$D_2 = \frac{(1+\nu(k-2)-\nu k\omega)}{2I_r(1+\nu)^{k-1}}. \tag{55}$$

The general solution of the differential Eq. (53) can be expressed as:

$$u(r) = r^{-k\omega}\left[C_2 - \int_1^r \rho^{k\omega}\left(D_1\left(\sigma_\theta^* - P_0^*\right) + D_2\left(\sigma_\theta^*\right)^a\right)\mathrm{d}\rho\right] \tag{56}$$

in which $C_2$ is a constant that can be determined using the known displacement at the (EPB) and $\rho$ is an auxiliary integration variable.

Finally, the radial displacement is simply expressed in dimensionless form as follows:

$$\bar{u}(r) = I_r \frac{u(r)}{r^{-k\omega}}$$

$$= I_r \left[ u_{EPB} r_p^{k\omega} + \int_r^{r_p} \rho^{k\omega} \left( D_1 \left( \sigma_\theta^* - P_0^* \right) + D_2 \left( \sigma_\theta^* \right)^a \right) \mathrm{d}\rho \right]. \quad (57)$$

The integral of the right-hand side of Eq. (57) can be numerically evaluated. Otherwise, using the variable change $R = C_1 r^{-\frac{k}{\beta}}$, and after some derivations, a closed-form solution can be provided as a function of the generalized exponential integral function, $E_n(x) \equiv \int_1^\infty \mathrm{e}^{-xt} t^{-n} \mathrm{d}t$.

$$\bar{u}(r) = I_r \left( u_{\mathrm{EPB}} r_p^{k\omega} + \left( A_1 + A_2 - A_3 \right) \right) \quad (58)$$

where

$$A_1 = \frac{D_1 a^{\frac{\beta}{a}} \left( R_p r_p^{\frac{k}{\beta}} \right)^{-(\alpha+1)}}{-\frac{k}{\beta}(\alpha+1)} \left[ \frac{W_0(x) x^{\alpha+\frac{\beta}{a}}}{e^{\left(\alpha+\frac{\beta}{a}\right)W(x)}} \left( e^{(\alpha+1)W(x)} + \frac{\beta}{a} E_{-\left(\alpha+\frac{\beta}{a}\right)} \left( -(\alpha+1) W_0(x) \right) \right) \right]_R^{R_p} \quad (59)$$

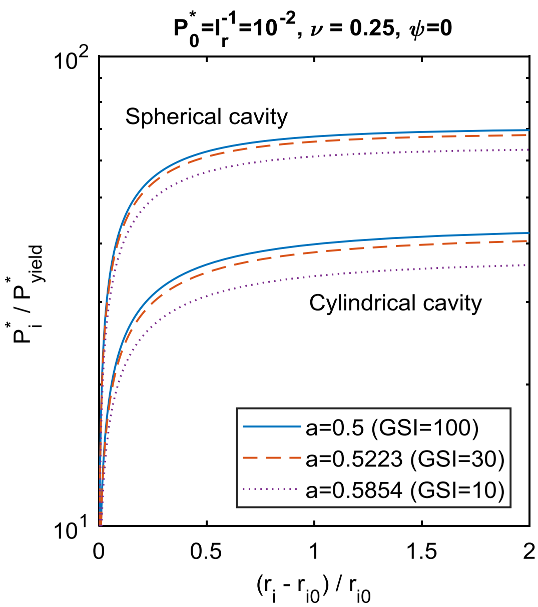


**Fig. 8** Typical cavity pressure–expansion curves adopting the large strain theory

$$A_2 = \frac{D_2 a^{\beta} \left( R_p r_p^{\frac{k}{\beta}} \right)^{-(\alpha+1)}}{-\frac{k}{\beta}(\alpha+1)} \left[ \frac{W_0(x) x^{\alpha+\beta}}{e^{(\alpha+\beta)W(x)}} \left( e^{(\alpha+1)W(x)} + \beta E_{-(\alpha+\beta)} \left( -(\alpha+1) W_0(x) \right) \right) \right]_R^{R_p}, \quad (60)$$

$$A_3 = \frac{D_1 P_0^*}{-\frac{k}{\beta}(\alpha+1)} \left( r_p^{k\omega+1} - r^{k\omega+1} \right) \quad (61)$$

in which $\alpha = -\frac{\beta}{k}(k\omega+1) - 1$.

Typical pressure–displacement curves for both cylindrical and spherical cavities are depicted in Fig. 7. For a given internal pressure $P_i^*$, the dimensionless displacement at cavity face increases with lowering dilatancy angle. It is also observed that the normalized load–displacement curves are almost identical when GSI > 30.

It should be emphasized that provided SST solutions are only valid for small expansions. Therefore, prediction of the theoretical limit pressure is not possible when adopting this theory.

(b) Large Strain Theory (LST)

To take into account the effect of large strain in the plastic zone, one can follow Chadwick (1959) in adopting the logarithmic strains expressed as follows:

$$\varepsilon_r = -\ln\left( \frac{\mathrm{d}r}{\mathrm{d}r_0} \right),, \quad (62)$$

$$\varepsilon_\theta = -\ln\left( \frac{r}{r_0} \right), \quad (63)$$

In the above equations, the index 0 is used to indicate the original length of a given radial distance $r$.

Substituting Eqs. (62) and (63) and the elastic strain formula given as per Eqs. (22) and (23) into the plastic flow rule expression (Eq. (50)) results in:

$$\ln\left( \left( \frac{r}{r_0} \right)^{k\omega} \left( \frac{\mathrm{d}r}{\mathrm{d}r_0} \right) \right) = D_1 P_0^* - D_1 \sigma_\theta^* - D_2 \left( \sigma_\theta^* \right)^a. \quad (64)$$

in which coefficients $D_1$ and $D_2$ are given, respectively, as per Eqs. (54) and (55). $\omega$ is the dilatancy parameter equal to $\frac{1-\sin(\psi)}{1+\sin(\psi)}$.

By means of the following change of variables:

$$R = C_1 r^{-\frac{k}{\beta}}, \quad (65)$$

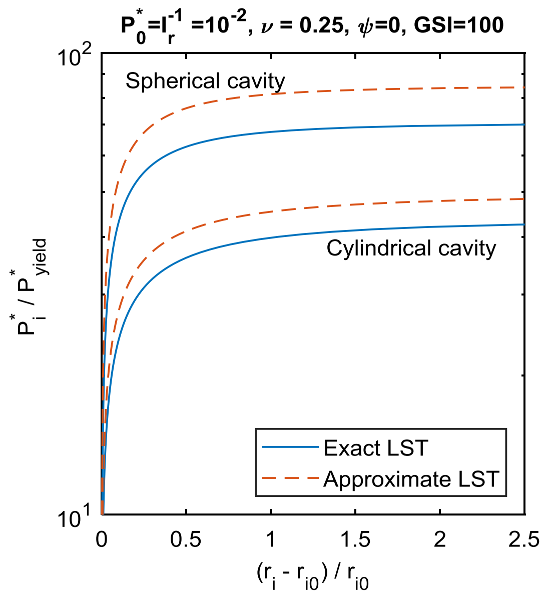


**Fig. 9** Comparison of cavity pressure–expansion curves computed by employing the approximate and exact solution according to large strain theory

$$\xi = \left(\frac{r_0}{r_p}\right)^{k\omega+1}. \tag{66}$$

Equation (64) is easily integrated over the interval $\left[r, r_p\right]$ leading to:

$$\eta\left[(1-\delta)^{k\omega+1} - \left(\frac{r_0}{r_p}\right)^{k\omega+1}\right] = -\int_R^{R_p} \frac{e^{D_1\sigma_\theta^* + D_2\left(\sigma_\theta^*\right)^a}}{R^{\frac{\beta(k\omega+1)}{k}+1}} \mathrm{d}R, \tag{67}$$

where

$$\delta = \frac{u_{(\mathrm{EPB})}}{r_p} = \frac{1}{2\mathrm{kI_r}}\left(P_{\mathrm{yield}}^* - P_0^*\right), \tag{68}$$

$$\eta = \frac{e^{D_1 P_0^*}\left(\beta\frac{(k\omega+1)}{k}\right)^{-1}}{R_p^{\beta\frac{(k\omega+1)}{k}}}. \tag{69}$$

By assuming $r_0 = r_{i0}$ and $r = r_i$, Eq. (67) is rewritten as follows:

$$\eta\left[(1-\delta)^{k\omega+1} - \Omega^{k\omega+1}\left(\frac{r_{i0}}{r_i}\right)^{k\omega+1}\right] = -\int_{R_i}^{R_p} \frac{e^{D_1\sigma_\theta^* + D_2\left(\sigma_\theta^*\right)^a}}{R^{\frac{\beta(k\omega+1)}{k}+1}} \mathrm{d}R, \tag{70}$$

where Ω is the inverse of the normalized plastic radius, i.e., Ω is expressed as per Eq. (47) as follows:

$$\Omega = \frac{r_i}{r_p} = \left(\frac{R_p}{R_i}\right)^{\frac{\beta}{k}}. \tag{71}$$

Finally, the following implicit relationship between the cavity pressure and the cavity expansion is obtained as follows:

$$\left(\frac{r_i}{r_{i0}}\right)^{k\omega+1} = \frac{\Omega^{k\omega+1}}{(1-\delta)^{k\omega+1} - \frac{1}{\eta}\int_{R_p}^{R_i} \frac{e^{D_1\sigma_\theta^* + D_2\left(\sigma_\theta^*\right)^a}}{R^{\frac{\beta(k\omega+1)}{k}+1}} \mathrm{d}R}. \tag{72}$$

Here, $r_i$ is the instant cavity radius and $r_{i0}$ is the original cavity radius before cavity expansion starts. The corresponding instant cavity volume $V_i$ and original volume $V_{i0}$ can be computed as:

$$\left(\frac{V_i}{V_{i0}}\right) = \left(\frac{r_i}{r_{i0}}\right)^{k+1}. \tag{73}$$

Typical pressure–expansion curves of both cylindrical and spherical cavities are depicted in Fig. 8 for different GSI values. It is observed that the pressure applied at the cavity wall does not increase indefinitely, but that a limit pressure is reached. This limit pressure denoted $P_{lim}^*$ can be found by putting $r_i/r_{i0} \to \infty$ in Eq. (72), i.e., $P_{lim}^*$ can be obtained implicitly from the following expression:

$$(1-\delta)^{k\omega+1} = \frac{1}{\eta}\int_{R_p}^{R_i} \frac{e^{D_1\sigma_\theta^* + D_2\left(\sigma_\theta^*\right)^a}}{R^{\frac{\beta(k\omega+1)}{k}+1}} \mathrm{d}R. \tag{74}$$

Note that $P_{lim}^*$ depends on five main parameters, which are the far field pressure $P_0^*$, the rigidity index $I_r = \frac{G}{\sigma_{ci} m_b^\beta}$, the Poisson's ratio $\nu$, the dilatancy angle $\psi$, and the exponent $a$ (i.e., GSI).

When $a = 0.5$ and by considering an incompressible material ($\nu = 0.5$) with no plastic volume change ($\psi = 0$), a closed-form solution of the limit pressure can be provided and the following holds:

$$P_{lim}^* = \left(\frac{W_0\left(C_3\right)}{2}\right)^2 + \frac{W_0\left(C_3\right)}{2}, \tag{75}$$

where,

$$C_3 = \frac{\left(\sqrt{4P^*_{y_{|a=0.5}} + 1} - 1\right) e^{\sqrt{4P^*_{y_{|a=0.5}} + 1} - 1}}{\left(1 - (1-\delta)^{k+1}\right)^{\frac{k}{k+1}}}. \tag{76}$$

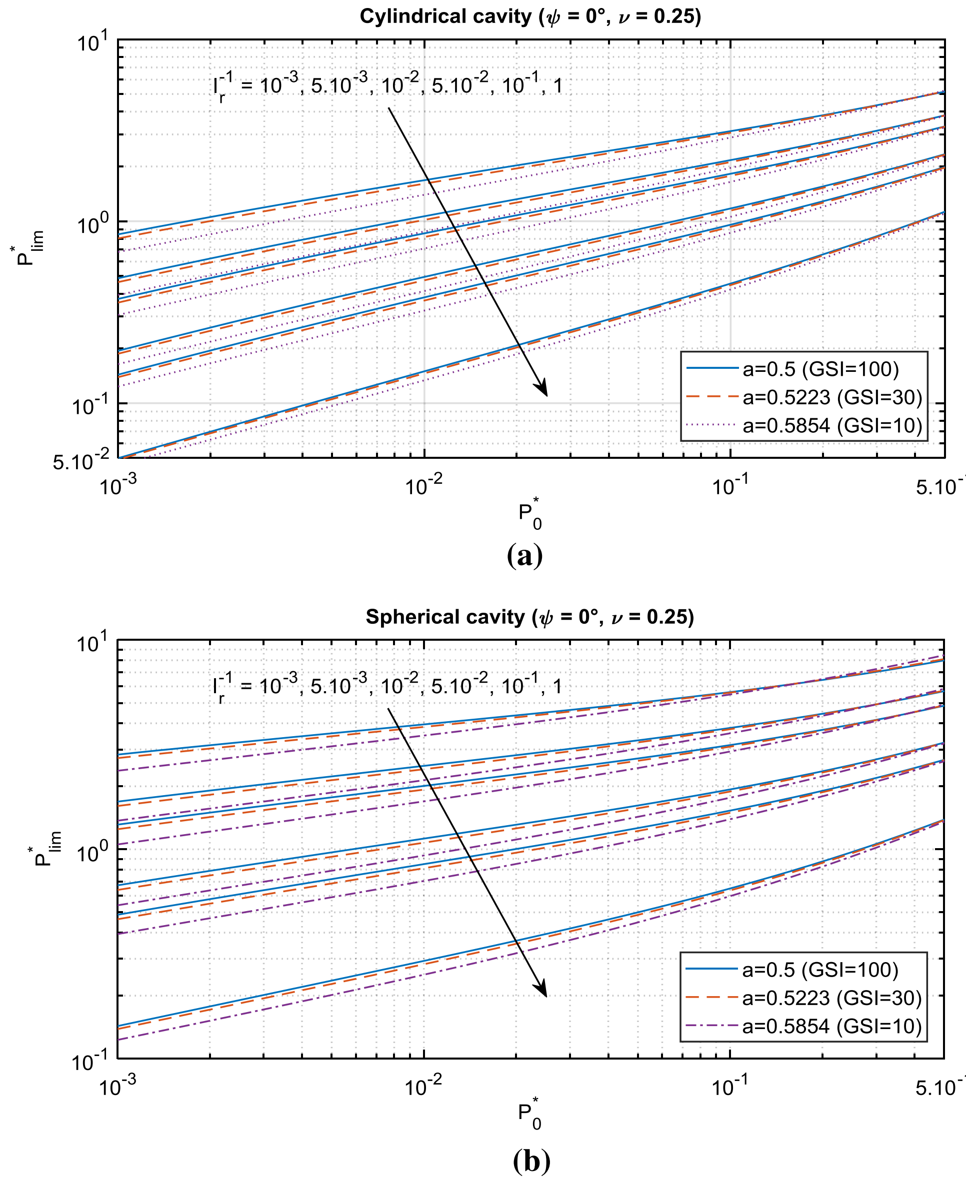


**Fig. 10** Limit pressure chart for cylindrical (**a**) and spherical (**b**) cavities

Furthermore, neglecting the contribution of elastic strains within the plastic region considerably simplifies the analysis of the cavity expansion problem. Indeed, the right-hand side of Eq. (64) vanishes. Hence, following the same procedure described above, a relatively simple expression for the relationship between the cavity pressure and the cavity expansion is obtained being exact for the special case of an elastically incompressible material with no plastic volume change:

$$\left(\frac{r_i}{r_{i0}}\right)^{k\omega+1} = \frac{\Omega^{k\omega+1}}{(1-\delta)^{k\omega+1} - \left(1 - \left(\frac{r_i}{r_p}\right)^{k\omega+1}\right)}. \tag{77}$$

Neglecting the contribution of elastic strains within the plastic region may seem to be a reasonable assumption since the elastic strains are considered to be much smaller than the plastic strains. This, however, does have a significant effect on the predicted results. Figure 9 depicts a comparison of the cavity pressure–displacement curves, which are computed according to both the exact and the approximate solutions. It can be noted that for the same $P_i^*/P_{yield}^*$, the evaluated radial displacement is larger when considering elastic strains.

## 6 Design Charts

Charts allowing easy and accurate estimation of the limit pressure for both cylindrical and spherical cavities are presented herein for $\psi = 0$ and $\nu = 0.25$. These charts provide a first aid to design engineers.

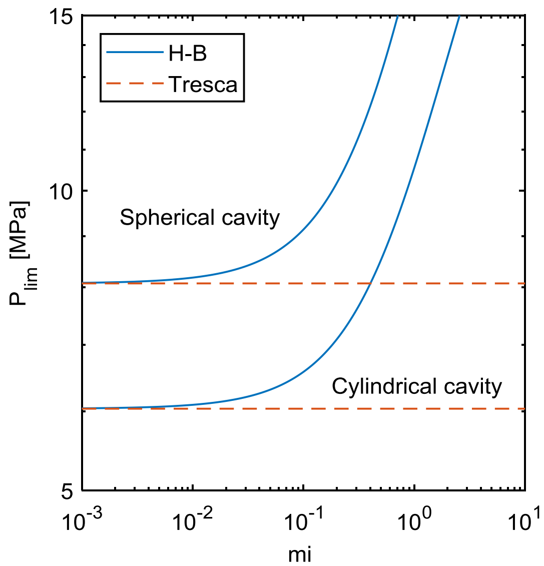


**Fig. 11** Limit pressure according to present work (exact solution Eq. 74) approaching that in a Tresca material when $m_i \rightarrow 0$

To cover the range of values likely to be encountered in practice, it is assumed that the far field pressure $P_0$ is comprised between 0 and 1[MPa] and that H–B core parameters are ranging as follows: $\sigma_{ci}$[MPa] $\in [1, 100]$., $m_i \in [1, 33]$, $D = 0$ and $GSI \in [10, 100]$. Thus, the scaled far field pressure $P_0^*$ evaluated as per Eq. (17) is ranging from $10^{-3}$ to $5.10^{-1}$. The values of the inverse rigidity index $I_r^{-1} = \left[10^{-3}, 5.10^{-3}, 10^{-2}, 5.10^{-2}, 10^{-1}, 1\right]$ will be used to compute the limit pressure values. As shown in Fig. 10, an increase of limit pressure as the far field stress and the shear modulus increase.

To illustrate the use of the provided charts, an example is given for computing the limit pressures of cylindrical and spherical cavities in a medium with a far field pressure $P_0$ of 100[kPa] consisting of an intact undisturbed H–B material ($D = 0$ and $GSI = 100$) with $m_i = 10$, $\sigma_{ci} = 10$[MPa], $G/\sigma_{ci} = 200$, $\psi = 0°$, and $\nu = 0.25$.

The H–B-derived parameters are $a = 0.5, m_b = 10$, and $s = 1$. The scaling parameter, $\beta = \frac{a}{1-a} = 1$. Then, the scaled far field pressure, $P_0^* = 1.1 \times 10^{-2}$ and $I_r^{-1} = 5 \times 10^{-2}$. Reading the scaled limit pressure from Fig. 10 for these input values, $P_{lim}^* = 0.59$ and 1.42, respectively, for cylindrical and spherical cavities. The corresponding limit pressure values can be computed as $P_{lim} = \left(P_{lim}^* - \frac{s}{m_b^{\beta/a}}\right)\sigma_{ci} m_b^\beta$ resulting in $P_{lim} = 58[MPa]$ and $141[MPa]$, respectively, for cylindrical and spherical cavities.

## 7 Validation

### 7.1 Comparison with Published Solutions

In the absence of published solutions of cavity expansion in an elastic–perfectly plastic H–B material, the presented solutions are validated for the case of H–B criterion reduced to Tresca criterion. Extensive literature is available on cavity expansion analyses for a material obeying the Tresca criterion (Yu 2000). The H–B failure criterion expression given as per Eq. (1) simply reduces to:

$$\sigma_1' = \sigma_3' + \sigma_{ci} s^a, m_b \rightarrow 0. \tag{78}$$

The above equation can be further written as:

$$\sigma_1' - \sigma_3' = \sigma_{ci} s^a = 2S_u, \tag{79}$$

where $S_u = \frac{\sigma_{ci} s^a}{2}$ denotes the undrained shear strength of the material. The limit pressure can be computed as (Yu 2000):

$$P_{lim} = P_0 + \left(\frac{4}{3}\right)^{k-1} S_u \left[1 + \ln\left(\frac{G}{S_u}\right) + \ln\left(\frac{1+\nu}{3(1-\nu)}\right)^{k-1}\right]. \tag{79}$$

For comparison matters, the following parameters are considered:$GSI = 100(a = 0.5)$, $m_i \rightarrow 0$, $\nu = 0.5$, $G/\sigma_{ci} = 300$ and $P_0/\sigma_{ci} = 0$. These rock mass parameters lead to an equivalent Tresca material with an undrained shear strength $S_u = \sigma_{ci}/2$.

The evolution of the scaled limit pressure as a function of a decreasing $m_i\left(m_i \rightarrow 0\right)$ for both cylindrical and spherical cavities is plotted in Fig. 11. It is found that the limit pressure values suggested by the present work are within 0.5% of those evaluated from the Tresca solutions (Yu 2000) when the strength parameter $m_i \leq 10^{-3}$.

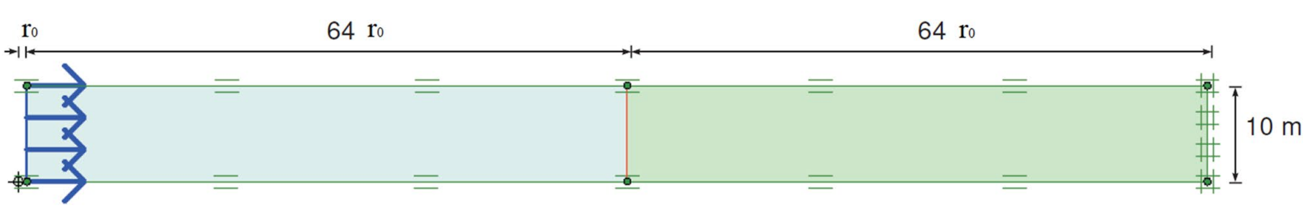


**Fig. 12** Geometry of the numerical model for cylindrical cavity expansion

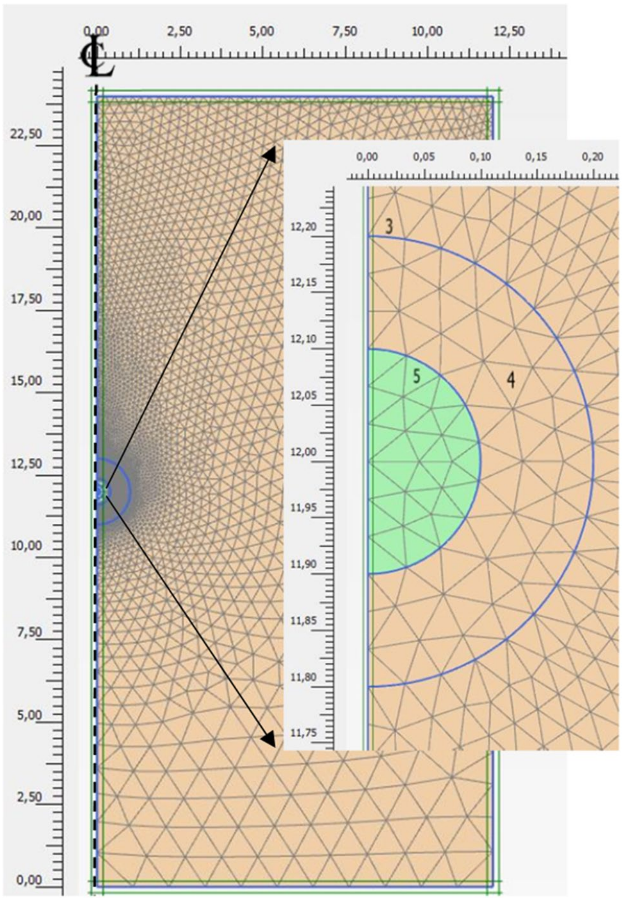

**Fig. 13** Geometry of the numerical model for cylindrical cavity expansion

## 7.2 Validation by Finite Element Method (FEM)

Using the finite element software, Plaxis.2018.0, a finite element analysis has been conducted to validate the analytical results. The geometry of the models as well as the selected boundary conditions for both spherical and cylindrical cavities are, respectively, shown in Figs. 12 and 13.

For the cylindrical cavity model, the initial cavity radius $r_0$ is set equal to 1 ml$m$. The width of the rock layer is selected to be 64 m extended by a correcting layer with 64 m width to simulate an infinite boundary (Burd and Houlsby 1990). The elastic properties of the correcting layer are $v'$ and $E'$. They were specified such that (Burd and Houlsby 1990):

$$\frac{1+v}{E} = \frac{\left(n^2-1\right)\left(1+v'\right)\left(1-2v'\right)}{E'\left(1+n^2(1-2v')\right)}; \quad n = 2. \tag{80}$$

For spherical cavity, a soil domain with a size of 12 m × 24 m was created with the mesh shown in Fig. 13. The spherical cavity has an initial radius $r_{i0} = 0.1$ m located at a depth of 12 m. It was found that the computational stability was enhanced by modelling the cavity as a linear elastic material; a nominal young modulus of 100 MPa and a Poisson's ratio of 0.2 were specified. The spherical cavity expansion is modeled by applying a positive volumetric strain to the cavity cluster allowing the cavity to expand. This modelling technique was employed successfully in previous studies employing Plaxis (Suryasentana and Lehane 2014; Suzuki and Lehane 2015; Xu 2007; Xu and Lehane 2008). It should be noted that the spherical cavity expansion is a relatively hard boundary value problem which consumes

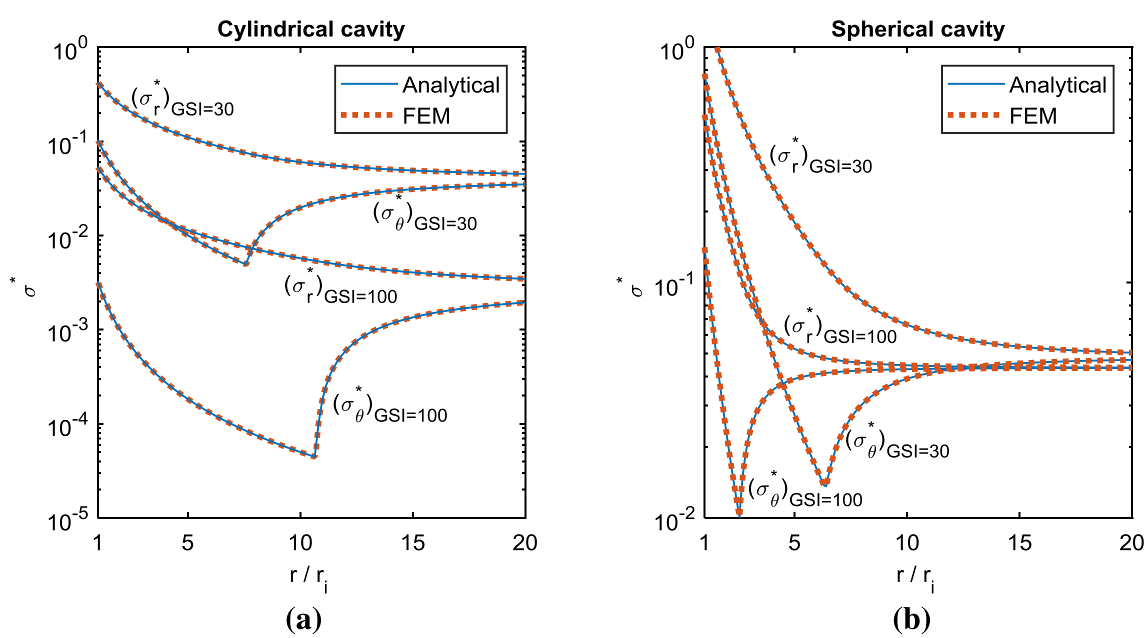


**Fig. 14** Radial distribution of radial and circumferential stresses: analytical vs FEM

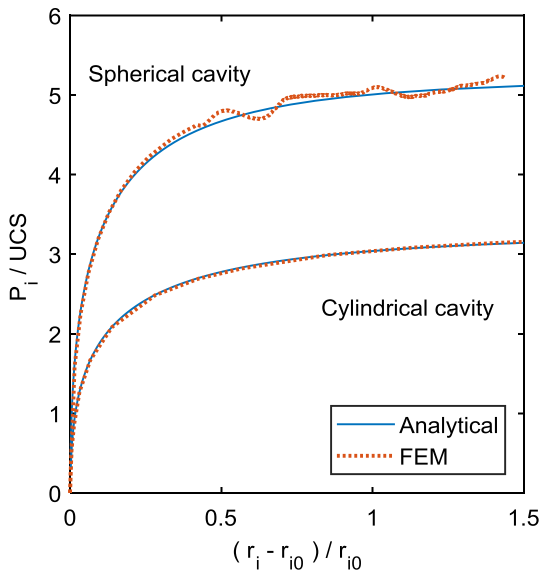


**Fig. 15** Cavity pressure against cavity wall displacement according to the analytical and finite element method

**Table 1** Comparison of limit pressure values by the analytical and finite element method

| $m_i$ | GSI | $P_{lim}$/UCS (cylindrical) | | Error (%) |
|---|---|---|---|---|
| | | Equation (74) | FEM | |
| 2 | 30 | 5.86 | 5.87 | 0.17 |
| | 50 | 5.81 | 5.76 | −0.86 |
| | 75 | 4.84 | 4.76 | −1.65 |
| | 100 | 3.27 | 3.27 | 0.00 |
| $m_i$ | GSI | $P_{lim}$/UCS (Spherical) | | Error (%) |
| | | Equation (74) | FEM | |
| 2 | 30 | 18.59 | 18.76 | 0.91 |
| | 50 | 13.38 | 13.48 | 0.74 |
| | 75 | 8.89 | 8.68 | −2.36 |
| | 100 | 5.22 | 5.21 | −0.19 |

a significant amount of computational power when solved using the finite element method.

The rock mass in the FEM model has properties similar to that of an undisturbed claystone (Evert Hoek 2006) ($D = 0$) with: $\sigma_{ci} = 25[\mathrm{MPa}]$, $m_i = 2$ and $E_i/\sigma_{ci} = 150$, and $GSI = [30, 50, 75, 100]$. The deformation modulus and the Poisson's ratio, which depend on GSI and $m_i$, are calculated according to Eqs. (7) and (8), respectively. The dilatancy angle is set equal to zero.

Note that the claystone is assumed to be weightless for the cylindrical cavity modelling while an initial isotropic stress $P_0$ of 240kPa is set for the spherical cavity modelling.

As shown in Figs. 14 and 15, analytical solutions of the present work are in excellent agreement with the FEM predictions. Besides, the limit pressure values computed by FEM are briefly summarized in Table 1 for both cylindrical and spherical cavities, with a graphic output (cf. Figure 15) corresponding to one simple case (GSI = 100). As can be seen, the cavity pressure–cavity expansion curves derived from analytical solutions and finite element method are in close agreement within 2%.

## 8 Conclusion

The expansion of cylindrical and spherical cavities in an infinite medium consisting of an elastic–perfectly plastic Hoek–Brown material is investigated. The use of a scaled form of the H–B failure criterion leads to considerable simplifications in defining the elasto-plastic response of the rock mass. Semi-analytical expressions are obtained for the stress and displacement fields. Although the solutions require some numerical integrations, they have the advantage of being highly robust considerably in comparison with other numerical techniques such as the finite element method. The analytical expressions were validated employing the finite element method.

The displacement field solution is derived by assuming a non-associated flow rule with a constant dilatancy angle. Solutions are developed based on both small and large strain theories. The internal pressure at the cavity wall increases indefinitely according to the small strain theory while it reaches a limit pressure when adopting large strain theory.

For practical purposes, design charts allowing easy and accurate estimation of the limit pressure for both cylindrical and spherical cavities are provided.

## Compliance with ethical standards

**Conflict of interest** The authors declare that there is no conflict of interest

## References


Brown Edwin T, Bray John W, Ladanyi Branko, Hoek Evert (1983) Ground response curves for rock tunnels. J Geotechn Eng 109(1):15–39

Burd HJ, Houlsby GT (1990) Finite element analysis of two cylindrical expansion problems involving nearly incompressible material behaviour. Int J Numer Anal Meth Geomech 14(5):351–366

Carranza-Torres C (2004) Elasto-plastic solution of tunnel problems using the generalized form of the Hoek–Brown failure criterion. Int J Rock Mech Min Sci 41:629–639

Carranza-Torres C, Fairhurst C (1999) The elasto-plastic response of underground excavations in rock masses that satisfy the

Hoek–Brown failure criterion. Int J Rock Mech Min Sci 36(6):777–809

Chadwick P (1959) The quasi-static expansion of a spherical cavity in metals and ideal soils. Q J Mech Appl Mech 12(1):52–71

Gibson RE, Anderson WF (1961) In situ measurement of soil properties with the pressuremeter. Civil Eng Public Works Rev 56(658):615–618

Hamdi S (2016) Pipe pile driving into rock. UCLouvain

Hoek E (2006) Practical-rock-engineering

Hoek E, Brown E (1980) Empirical strength criterion for rock masses. J Geotech Eng Div ASCE 106(GT9):1013–1035

Hoek E, Brown ETT (1997) Practical estimates of rock mass strength. Int J Rock Mech Min Sci 34(8):1165–1186

Hoek E, Diederichs MS (2006) Empirical estimation of rock mass modulus. Int J Rock Mech Min Sci 43(2):203–215

Hoek Evert, Carranza Carlos, Corkum Brent (2002) Hoek–Brown failure criterion—2002 Edition. Narms-Tac 1:267–273

Londe Pierre (1988) Discussion of 'determination of the shear failure envelope in rock masses' by Roberto Ucar (March, 1986, Vol. 112, No. 3). J Geotech Eng 114(3):374–376

Randolph MF, Wroth CP (1979) An analytical solution for the consolidation around a driven pile. Int J Numer Anal Meth Geomech 3(3):217–229

Rojat Fabrice, Labiouse Vincent, Mestat Philippe (2015) Improved analytical solutions for the response of underground excavations in rock masses satisfying the generalized Hoek–Brown failure criterion. Int J Rock Mech Min Sci 79:193–204

Salgado R, Mitchell JK, Jamiolkowski M (1997) Cavity expansion and penetration resistance in sand. J Geotech Geoenviron Eng 123(4):344–354

Serrano A, Olalla C, Reig I (2011) Convergence of circular tunnels in elastoplastic rock masses with non-linear failure criteria and non-associated flow laws. Int J Rock Mech Min Sci 48(6):878–887

Sharan SK (2003) Elastic–Brittle–Plastic analysis of circular openings in Hoek–Brown media. Int J Rock Mech Min Sci 40(6):817–824

Sharan SK (2005) Exact and Approximate Solutions for Displacements around Circular Openings in Elastic–Brittle–Plastic Hoek-Brown Rock. Int J Rock Mech Min Sci 42(4):542–549

Sharan SK (2008) Analytical Solutions for Stresses and Displacements around a Circular Opening in a Generalized Hoek-Brown Rock. Int J Rock Mech Min Sci 45(1):78–85

Suryasentana SK, Lehane BM (2014) Numerical derivation of CPT-based p–y curves for piles in sand. Géotechnique 64(3):186–194

Suzuki Y, Lehane BM (2015) Analysis of CPT end resistance at variable penetration rates using the spherical cavity expansion method in normally consolidated soils. Comput Geotech 69(69):141–152

Vásárhelyi B (2009) A possible method for estimating the Poisson's rate values of the rock masses. Acta Geodaetica et Geophysica Hungarica 44(3):313–322

Vesic AS (1973) Expansion of cavities in infinite soil mass (closure). J Soil Mech Found Div 99(sm5):409

Wang Yarlong (1996) Ground response of circular tunnel in poorly consolidated rock. J Geotech Eng 122(9):703–708

Xu X (2007) Investigation of the end bearing performance of displacement piles in sand. The University of Western Australia, Perth

Xu X, Lehane BM (2008) Pile and penetrometer end bearing resistance in two-layered soil profiles. Géotechnique 58(3):187–197

Yasufuku N, Hyde AFL (1995) Pile end-bearing capacity in crushable sands. Géotechnique 45(4):663–676

Ypma Tjalling J (1995) Historical development of the newton-raphson method. SIAM Rev 37(4):531–551

Yu HS (2000) Elastic-perfectly plastic solutions. Cavity Expansion Methods in Geomechanics. Springer, Dordrecht, pp 32–94